JOURNAL OF MAGNETIC RESONANCE **124,** 279–285 (1997)
ARTICLE NO. MN961059

Two-Dimensional Multiple-Quantum MAS NMR of Quadrupolar Nuclei. Acquisition of the Whole Echo

STEVEN P. BROWN AND STEPHEN WIMPERIS

Physical Chemistry Laboratory, University of Oxford, South Parks Road, Oxford OX1 3QZ, United Kingdom

Received November 12, 1996

Frydman and Harwood have shown that a combination of the experimental techniques of magic-angle spinning (MAS) and two-dimensional multiple-quantum NMR can be used to remove the second-order quadrupolar broadening of the central transition of half-integer nuclear spins ($I = \frac{3}{2}, \frac{5}{2}$, etc.) (*1, 2*). Since its introduction in only 1995, this approach has already gained widespread popularity and has been used to measure chemical and second-order isotropic shifts in a range of quadrupolar nuclei, including ^{11}B, ^{23}Na, ^{87}Rb ($I = \frac{3}{2}$) and ^{17}O, ^{27}Al, ^{55}Mn ($I = \frac{5}{2}$) (*1–8*). Indeed, it seems likely that, owing to its experimental simplicity and often excellent resolution, this new method will largely supplant the older techniques of double rotation (DOR) (*9*) and dynamic angle spinning (DAS) (*10, 11*).

Several modifications and improvements to the original multiple-quantum MAS experiment have recently been presented. Fernandez and Amoureux have shown that pure absorption-mode lineshapes can be achieved by combining the echo and antiecho coherence-transfer pathways in the same manner as that widely used in liquid-state two-dimensional NMR (*3, 5*). Brown *et al.* have also adopted this approach and have used a split multiple-quantum/single-quantum evolution (t_1) period to obtain complete refocusing of the second-order quadrupolar broadening in the F_1 dimension of the two-dimensional spectrum (*8*). Meanwhile, Massiot *et al.* have taken a different approach to pure absorption-mode lineshapes and, following on from the DAS work of Grandinetti *et al.* (*12*), have demonstrated a multiple-quantum MAS experiment based on acquisition of the whole coherence-transfer echo (*6*). This last method is reminiscent of techniques widely used in magnetic resonance imaging (MRI) (*13*).

The purpose of this Communication is to discuss the advantages of using whole-echo acquisition in the multiple-quantum MAS experiment and, in particular, to show that this approach to pure absorption-mode lineshapes is especially suitable for use in combination with a split multiple-quantum/single-quantum evolution (t_1) period. We present experiments that differ from those of Massiot *et al.* (*6*) only in the manner in which the free-precession periods are defined. As a result, both the sensitivity and the resolution are unchanged. Our new experiments, however, have the following favorable properties: (i) the acquisition (t_2) period can be kept very short, thereby minimizing the introduction of noise; (ii) time-domain weighting functions are easily applied; and (iii) shearing and/or time-dependent first-order phase correction of the data are not required.

Figure 1a shows the pulse sequence and coherence-transfer pathway diagram (*14*) used by Massiot *et al.* for recording triple-quantum MAS spectra (*6*). Phase cycling can be used to select either $p = +3$ or -3 coherence during the evolution period, t_1. The τ period and the final (refocusing) pulse ensure that a symmetrical or whole echo is detected in the acquisition period, t_2, even when $t_1 = 0$ (*12*). A whole echo has the property that its Fourier transform does not contain any dispersion-mode components (*13*), and therefore, this experiment yields pure absorption-mode lineshapes even though only a single-coherence pathway is selected during t_1. For the whole-echo method to be successful, however, the inhomogenous second-order quadrupolar broadening must dominate the homogeneous broadening (*6, 12*). Otherwise, relaxation will lead to echoes with asymmetric envelopes and these will yield partly dispersion-mode lineshapes.

To review the theory behind this experiment, we will start by considering a system where the nucleus has spin quantum number $I = \frac{3}{2}$, the asymmetry parameter, η, of the quadrupolar interaction is zero, and a single crystallite, rather than a powder, is present. The orientation of the principal axis of the quadrupolar interaction with respect to the rotor axis is described by an angle χ. In this case, the MAS-averaged second-order quadrupolar frequency shifts for the central transition and the triple-quantum coherence can be given in the notation of Brown *et al.* (*8*) as

$$\Omega^{(2)}_{p=\pm1} = \pm A(7 - 27\,B), \qquad [1a]$$

$$\Omega^{(2)}_{p=\pm3} = \pm A(-21 + 21\,B), \qquad [1b]$$

where

$$A = \frac{2\omega_Q^2}{35\omega_0}, \qquad [2a]$$

1090-7807/97 $25.00

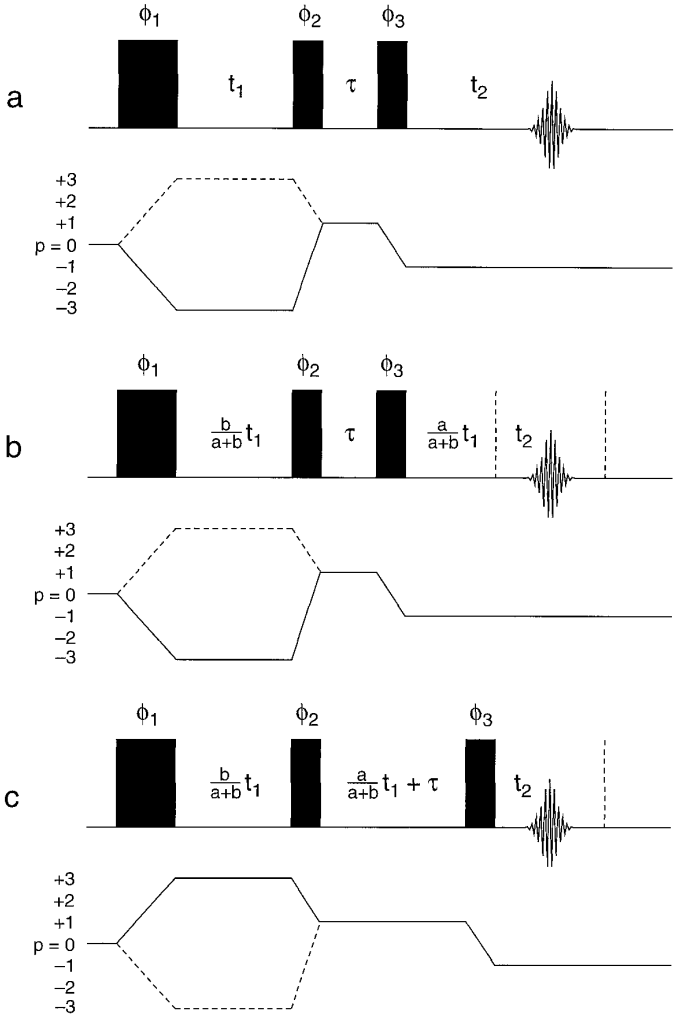

FIG. 1. Pulse sequences and coherence-transfer pathway diagrams for two-dimensional triple-quantum MAS NMR experiments with acquisition of the whole echo. The experiment in (a) is that used by Massiot *et al.* (*6*) while the new experiments in (b, c) are discussed in the text. The vertical dotted lines in (b, c) indicate the limits of the acquisition period, t_2. For spin $I = \frac{3}{2}$ nuclei, the coherence-transfer pathways shown as solid lines should be selected using phase cycling while, for spin $I = \frac{5}{2}$ nuclei, the pathways shown as dashed lines should be selected. Consideration of the efficiency of coherence transfer achievable with soft pulses leads us to believe that the pulse sequence in (b) is the method of choice for spin $I = \frac{5}{2}$ nuclei and that in (c) for spin $I = \frac{3}{2}$ nuclei. Phase-cycling schemes for the pulse phases ϕ_1, ϕ_2, and ϕ_3 and for the receiver phase ϕ_R are discussed by Massiot *et al.* in Ref. (*6*).

$$B = d^4_{0,0}(\chi)d^4_{0,0}(54.7°). \quad [2b]$$

The corresponding first-order quadrupolar frequency shifts, $\Omega^{(1)}_{p=\pm1}$ and $\Omega^{(1)}_{p=\pm3}$, are all zero. Thus, for a single crystallite spinning at the magic angle (54.7°), there are isotropic quadrupolar frequency shifts of $-7A$ and $21A$, as well as anisotropic frequency shifts of $27AB$ and $-21AB$, for the $p = -1$ central transition and $p = -3$ triple-quantum coherence, respectively. In a powdered sample, a spherical average over all values of the angle χ must be considered and the resulting continuous distribution of anisotropic frequency shifts will appear as an inhomogeneous second-order quadrupolar broadening.

If the $p = -3$ pathway is selected during t_1 (solid lines in Fig. 1a), the detected signal for the experiment used by Massiot *et al.* (*6*) has the form

$$s(t_1, t_2) = \exp\{-iA(21 - 21B)t_1\} \times \exp\{-iA(-7 + 27B)(t_2 - \tau)\}, \quad [3]$$

where the homogeneous broadening (transverse relaxation) and the chemical shift have been neglected. The anisotropic frequency shifts are refocused when

$$t_2 = \tau + \frac{21}{27}t_1 = \tau + \frac{7}{9}t_1. \quad [4]$$

Thus, in a powdered sample, an echo will form in the acquisition period at the point given by Eq. [4]. The duration of the period τ must be greater than half of the echo duration so that, as mentioned above, the symmetry of the echo envelope is not broken when $t_1 = 0$ (*6, 12*).

As t_1 is incremented during the two-dimensional experiment, Eq. [4] shows that the echo forms later and later in the acquisition period. Grandinetti *et al.* (*12*) and Massiot *et al.* (*6*) have discussed the problem of applying a weighting function to this data and have suggested using a time-shifted Gaussian function that tracks the echo through the acquisition period, t_2. After two-dimensional Fourier transformation, the inhomogeneous second-order broadening is spread out along a ''ridge'' (*15*) which has a slope of $-\frac{7}{9}$ with respect to the F_2 axis. The slope is a direct consequence of Eq. [4]. This is not the desired format for the spectrum, however, and it has become standard practice to shear the data such that the inhomogeneously broadened ridges appear parallel to the F_2 axis. A projection of the spectrum onto the F_1 axis then yields a purely isotropic spectrum. Grandinetti *et al.* (*12*) and Massiot *et al.* (*6*) have shown that this shearing is best performed in the time domain by applying a t_1-dependent first-order phase correction to the data after the Fourier transformation with respect to t_2. Simultaneously, they also apply a τ-dependent first-order phase correction to remove the phase distortion that results from the top of the echo not coinciding with $t_2 = 0$ when $t_1 = 0$.

As discussed by Massiot *et al.* (*6*), it is also possible to select the $p = +3$ pathway during t_1 (dashed lines in Fig. 1a). In this case, the detected signal has the form

$$s(t_1, t_2) = \exp\{+iA(21 - 21B)t_1\} \times \exp\{-iA(-7 + 27B)(t_2 - \tau)\}, \quad [5]$$

and the refocusing of the inhomogeneous broadening occurs when

$$t_2 = \tau - \frac{7}{9} t_1. \qquad [6]$$

Equation [6] shows that the (anti)echo forms earlier and earlier in the acquisition period as t_1 is incremented. Therefore, the τ period must be much longer than in the $p = -3$ version of the experiment so that the symmetry of the echo envelope is not broken when t_1 reaches its maximum value. This means that the $p = -3$ version of the experiment is to be preferred since signal loss through relaxation will clearly be less during the shorter τ period. Apart from taking into account the different signs in Eqs. [4] and [6], the same data processing is used with both versions of the experiment.

The processing procedures used by Massiot *et al.* (*6*) to apply time-shifted Gaussian weighting functions, to shear the inhomogeneously broadened ridges, and to correct the τ-dependent phase become unnecessary if the modified multiple-quantum MAS experiment of Fig. 1b is used. This experiment is identical to that in Fig. 1a except that the evolution and acquisition periods, t_1 and t_2, have been defined differently, with the t_1 period split between evolution of triple- and single-quantum coherence in the manner of Brown *et al.* (*8*). If the $p = -3$ pathway is selected during the first part of t_1 (solid lines in Fig. 1b), the detected signal for this experiment has the form

$$\begin{aligned} s(t_1, t_2) &= \exp\left\{ -iA(21 - 21B)\frac{bt_1}{a+b} \right\} \\ &\quad \times \exp\left\{ -iA(-7 + 27B)\left(t_2 + \frac{at_1}{a+b} - \tau \right) \right\} \\ &= \exp\left\{ -iA[7(3b - a) + 3(9a - 7b)B]\frac{t_1}{a+b} \right\} \\ &\quad \times \exp\left\{ -iA(-7 + 27B)(t_2 - \tau) \right\}, \end{aligned} \qquad [7]$$

and if the parameters describing the division of the t_1 period are chosen as $a = 7$ and $b = 9$, Eq. [7] becomes

$$\begin{aligned} s(t_1, t_2) &= \exp\left\{ -i\frac{35}{4} At_1 \right\} \\ &\quad \times \exp\{ -iA(-7 + 27B)(t_2 - \tau) \}. \end{aligned} \qquad [8]$$

Only an isotropic second-order frequency shift is now present in the modulation as a function of t_1. Therefore, shearing of the final spectrum is unnecessary as the inhomogeneously broadened ridge is already parallel to F_2 (*8*).

In the experiment of Fig. 1b, Eq. [8] shows that the echo forms when

$$t_2 = \tau \qquad [9]$$

and hence always forms at the same point in the acquisition period. This confers several practical advantages. It means that the acquisition period can be much shorter than in the experiment of Fig. 1a, thereby keeping the introduction of noise to a minimum. It also means that the same simple weighting function can be applied to all the acquired free-induction decays. For optimum sensitivity, the best position within the acquisition window to form the echo is at its center, that is, to have $\tau = \frac{1}{2} t_2^{\max}$ as shown in Fig. 1b. This means that the need for the explicit τ-dependent first-order phase correction used by Massiot *et al.* (*6*) is obviated as one of two computationally simpler corrections can be made. As shown in Fig. 2, either the time origin of the discrete Fourier transform can be moved to the center of the echo or, after a conventional Fourier transformation with respect to t_2, alternate data points can be inverted (*16*).

Even with the highest radiofrequency power amplification currently available, the pulses used in multiple-quantum MAS experiments on half-integer quadrupolar nuclei are almost always ''soft'' or ''weak.'' That is, the inherent nutation rate of the pulse, $\omega_1 = -\gamma B_1$, is usually small compared to a typical quadrupole coupling parameter, ω_Q. This is not a disadvantage for the first and third pulses in the experiments of Fig. 1 where efficient direct excitation of triple-quantum coherence and selective refocusing of the inhomogeneous second-order broadening of the central transition are only possible because $|\omega_1| \ll |\omega_Q|$ (*17, 18*). However, the weakness of the second pulse in the experiments of Fig. 1 represents a major disadvantage as it results in the efficiency of coherence transfer between the $p = \pm 3$ pathways and the $p = +1$ pathway being poor, thereby greatly reducing the sensitivity of the experiment. Figure 3 shows plots of the calculated efficiency of coherence transfer between coherence orders $p = +3$ and $p = +1$ (solid line) and $p = -3$ and $p = +1$ (dashed line) for spin $I = \frac{3}{2}$ over a range of values of the pulse flip angle $\beta = |\omega_1| t_p$ and of the ratio $|\omega_1/\omega_Q|$. The plots show that, as expected, the efficiency of coherence transfer falls rapidly as the ratio $|\omega_1/\omega_Q|$ decreases. However, they also show that, when $|\omega_1| < |\omega_Q|$, the efficiency of coherence transfer between $p = +3$ and $p = +1$ is greater than that between $p = -3$ and $p = +1$ for most flip angles. This reflects the well-known result that the larger the change in coherence order, p, the more difficult efficient coherence transfer is to achieve.

For use on a spin $I = \frac{3}{2}$ nucleus, both the $p = -3$ version of the experiment in Fig. 1a (i.e., the preferred version with

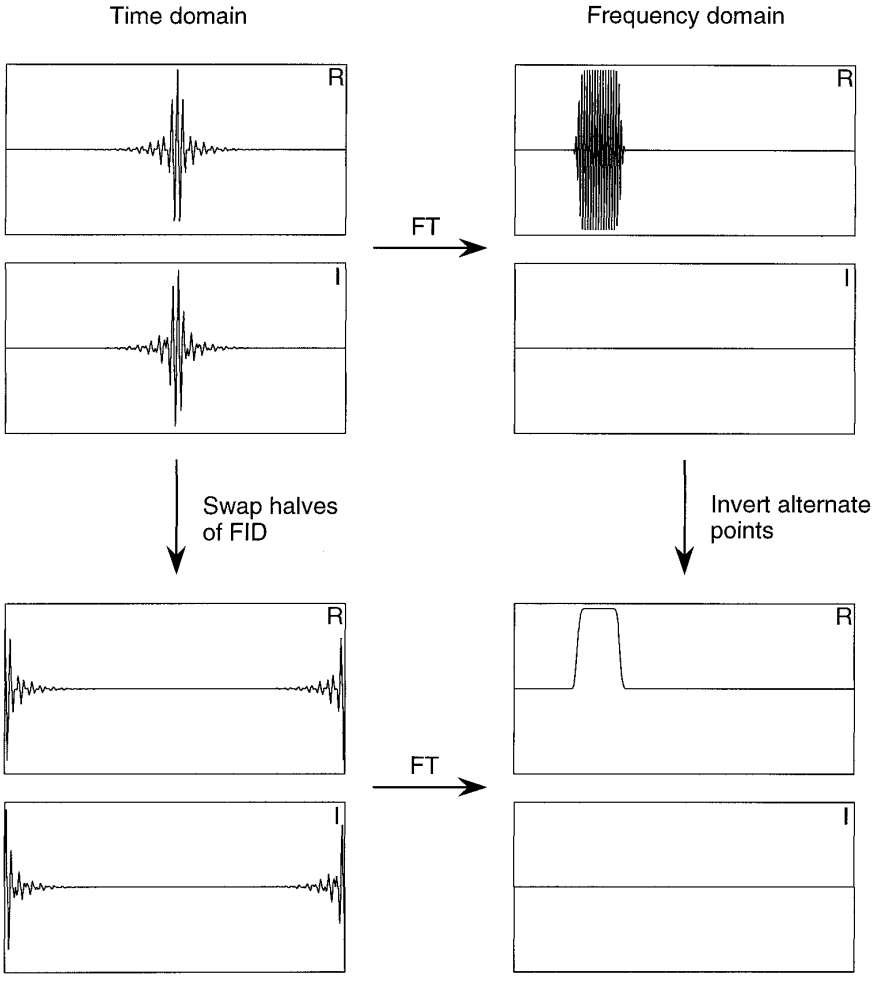

FIG. 2. Discrete Fourier transformation of a whole echo to yield a purely real lineshape. The real (R) and imaginary (I) parts of the echo are shown at the top left. Note that the real part is symmetric and the imaginary part antisymmetric about the top of the echo. If the echo is in the center of the acquisition window, then Fourier transformation yields a purely real, absorption-mode lineshape, but one where there is a 180° phase difference between adjacent points. This can be corrected by inverting the sign of alternate data points to yield the desired spectrum shown at bottom right. The same result can be achieved by redefining the time origin of the Fourier transform to be the top of the echo.

the shorter τ period) and the experiment in Fig. 1b involve coherence transfer between the $p = -3$ and $p = +1$ pathways. To achieve greater coherence-transfer efficiency, therefore, we introduce the new triple-quantum MAS experiment in Fig. 1c in which the second part of the split t_1 period precedes the τ period rather than the acquisition period. If the $p = +3$ pathway is selected during the first part of t_1 (solid lines in Fig. 1c), the detected signal for this experiment has the form

$$s(t_1, t_2) = \exp\left\{ +iA(21 - 21B)\frac{bt_1}{a+b} \right\} \times \exp\left\{ -iA(-7 + 27B)\left(t_2 - \frac{at_1}{a+b} - \tau \right) \right\}$$

$$= \exp\left\{ +iA[7(3b - a) + 3(9a - 7b)B]\frac{t_1}{a+b} \right\} \times \exp\{ -iA(-7 + 27B)(t_2 - \tau) \}, \quad [10]$$

and if $a = 7$ and $b = 9$, Eq. [10] becomes

$$s(t_1, t_2) = \exp\left\{ +i\frac{35}{4}At_1 \right\} \times \exp\{ -iA(-7 + 27B)(t_2 - \tau) \}. \quad [11]$$

Thus, apart from a change in the apparent sense of precession during t_1, this experiment yields an identical result to the

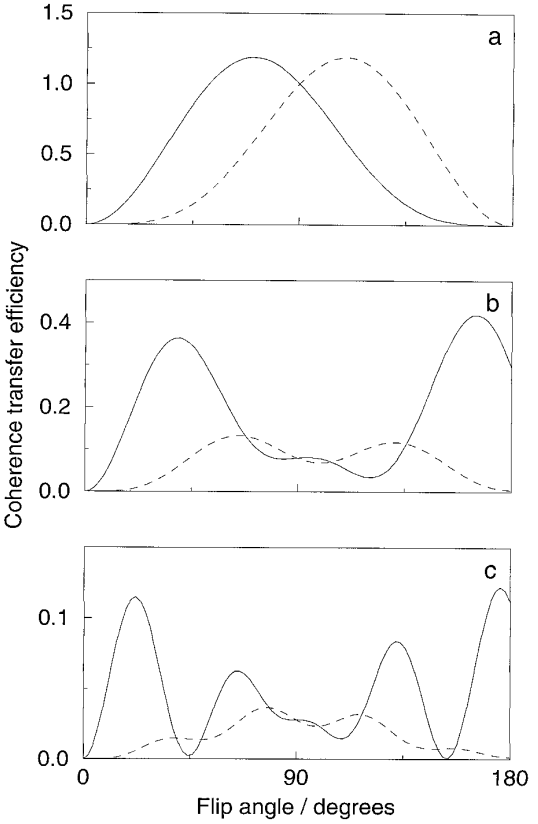

FIG. 3. Calculated efficiency of coherence transfer between coherence orders $p = +3$ and $+1$ (solid line) and $p = -3$ and $+1$ (dashed line) for a spin $I = \frac{3}{2}$ nucleus over a range of values of the pulse flip angle $\beta = |\omega_1|t_p$. The ratio $|\omega_Q/\omega_1|$ is 0.0 in (a), 2.0 in (b), and 4.0 in (c). The amplitude of the coherence transfer has been normalized such that it is equal to 1.0 for a ''hard'' 90° pulse. Since the longest pulse of this type that we apply in the present experiments (2.1 μs) is much shorter than a typical rotor period ($\sim$190 μs), these calculations were performed assuming a nonspinning sample.

experiment in Fig. 1b and retains the advantages of having short τ and t_2 periods and a stationary whole echo that, if $\tau = \frac{1}{2}t_2^{\max}$, is formed in the middle of the acquisition window. The advantage of the experiment in Fig. 1c over that in Fig. 1b and the $p = -3$ version in Fig. 1a is that the change in coherence order produced by the second pulse is $\Delta p = -2$ rather than $\Delta p = +4$. For spin $I = \frac{3}{2}$ nuclei, therefore, we believe that the experiment in Fig. 1c is the method of choice as a triple-quantum MAS experiment with whole-echo acquisition.

For a spin $I = \frac{5}{2}$ nucleus and for a single crystallite with asymmetry parameter $\eta = 0$, the MAS-averaged second-order quadrupolar frequency shifts for the central transition and the triple-quantum coherence are given by (*19*)

$$\Omega^{(2)}_{p=\pm1} = \pm\frac{2A}{3}(28 - 108B), \qquad [12a]$$

$$\Omega^{(2)}_{p=\pm3} = \pm\frac{2A}{3}(21 - 171B), \qquad [12b]$$

where A and B are as given in Eq. [2]. In the experiment of Fig. 1a, if the $p = +3$ pathway is selected during t_1 (dashed lines), the detected signal has the form

$$s(t_1, t_2) = \exp\left\{-i\frac{2A}{3}(21 - 171B)t_1\right\} \times \exp\left\{-i\frac{2A}{3}(-28 + 108B)(t_2 - \tau)\right\}, \qquad [13]$$

and the second-order quadrupolar echo occurs at the point

$$t_2 = \tau + \frac{171}{108}t_1 = \tau + \frac{19}{12}t_1. \qquad [14]$$

For a spin $I = \frac{5}{2}$ nucleus, therefore, it is selection of the $p = +3$ pathway that produces an echo that forms later and later in the acquisition period as t_1 increases and means that, in the experiment of Fig. 1a, a short τ period can be used. Similarly, in the experiments in Figs. 1b and 1c, the opposite triple-quantum coherence order to that used for spin $I = \frac{3}{2}$ must also be selected during the first part of the t_1 period, as shown by the dashed coherence pathways. This change in coherence pathway means that, for spin $I = \frac{5}{2}$, the $p = +3$ experiment of Fig. 1b becomes the whole-echo triple-quantum MAS experiment of choice since the change in coherence order produced by the second pulse is $\Delta p = -2$ as opposed to $\Delta p = +4$. Note that the constants a and b also change their values for spin $I = \frac{5}{2}$ experiments to $a = 19$ and $b = 12$.

Experiments were performed on a Bruker MSL 400 spectrometer using a commercial 7 mm MAS probehead. All pulses were generated with the highest achievable gain of the Bruker 1 kW broadband radiofrequency power amplifier. Two samples were used: (i) an equal mixture of sodium oxalate, $Na_2C_2O_4$, and sodium sulfate, Na_2SO_4, for ^{23}Na NMR at 105.8 MHz, and (ii) albite (Oxford University Museum, OUM 9408), $NaSi_3AlO_8$, for ^{27}Al NMR at 104.2 MHz. The MAS speed was approximately 5.3 kHz. The experiment of Fig. 1c was used for the ^{23}Na ($I = \frac{3}{2}$) NMR and that of Fig. 1b for the ^{27}Al ($I = \frac{5}{2}$) NMR. In each experiment, a 96-step phase cycle was used to select the solid coherence-transfer pathways, as described in detail by Massiot *et al.* (*6*). These phase cycles consisted of 12 steps to select either $\Delta p = +3$ or -3 with the first pulse and 8 steps to select $\Delta p = -2$ with the third pulse. Note that neither the States–Haberkorn–Ruben (hypercomplex) (*20*) nor TPPI (*21*) methods for sign discrimination in F_1 are

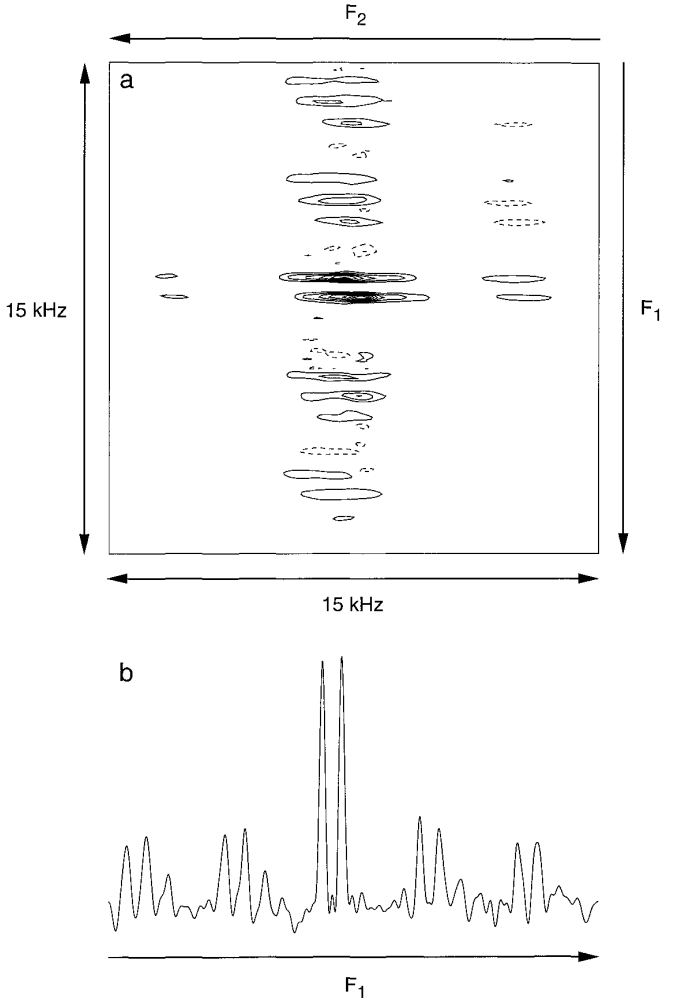

FIG. 4. Two-dimensional triple-quantum MAS ^{23}Na NMR spectrum of an equal mixture of sodium oxalate, $Na_2C_2O_4$, and sodium sulfate, Na_2SO_4, recorded using the experiment in Fig. 1c with $a = 7$ and $b = 9$. The contour plot is shown in (a) and the projection onto F_1 in (b). The full F_1 and F_2 spectral widths were 15 and 50 kHz, 192 transients (consisting of 256 points each) were averaged for each of the 64 increments of t_1, and the relaxation interval was 1 s. Total experiment duration was ~4 hours. The length of the triple-quantum excitation pulse was 6.1 μs, of the $p = +3$ to $+1$ transfer pulse was 2.1 μs, and of the selective refocusing pulse was 4.0 μs. The τ period was 1.33 ms ($7 \times$ rotor period). The data were zero filled to 1024 points in t_1 and 512 points in t_2 prior to Fourier transformation.

necessary in this type of experiment since the sign information is inherent in the selection of a single-coherence pathway in t_1.

Figure 4 shows a contour plot of a 15 by 15 kHz region of the two-dimensional triple-quantum MAS ^{23}Na NMR spectrum of the sulfate/oxalate sample recorded using the experiment in Fig. 1c (with selection of the solid coherence pathway). The isotropic spectrum obtained by projection of the two-dimensional spectrum onto the F_1 axis is also shown. The two distinct ^{23}Na sites are easily distinguished. Note the presence of spinning sidebands in both the F_2 and, especially, F_1 dimensions. The pattern of spinning sidebands in F_1 is complex and will be discussed elsewhere. The time-domain data were processed by (i) symmetric zero filling of the echoes in t_2, (ii) applying a simple symmetric Gaussian weighting function in t_2, (iii) redefining the time origin of the discrete Fourier transform as in Fig. 2, (iv) complex Fourier transforming with respect to t_2, (v) conventional zero filling in t_1, and then (vi) complex Fourier transforming with respect to t_1.

Figure 5 shows a contour plot and F_1 projection of a 10 by 10 kHz region of the two-dimensional triple-quantum

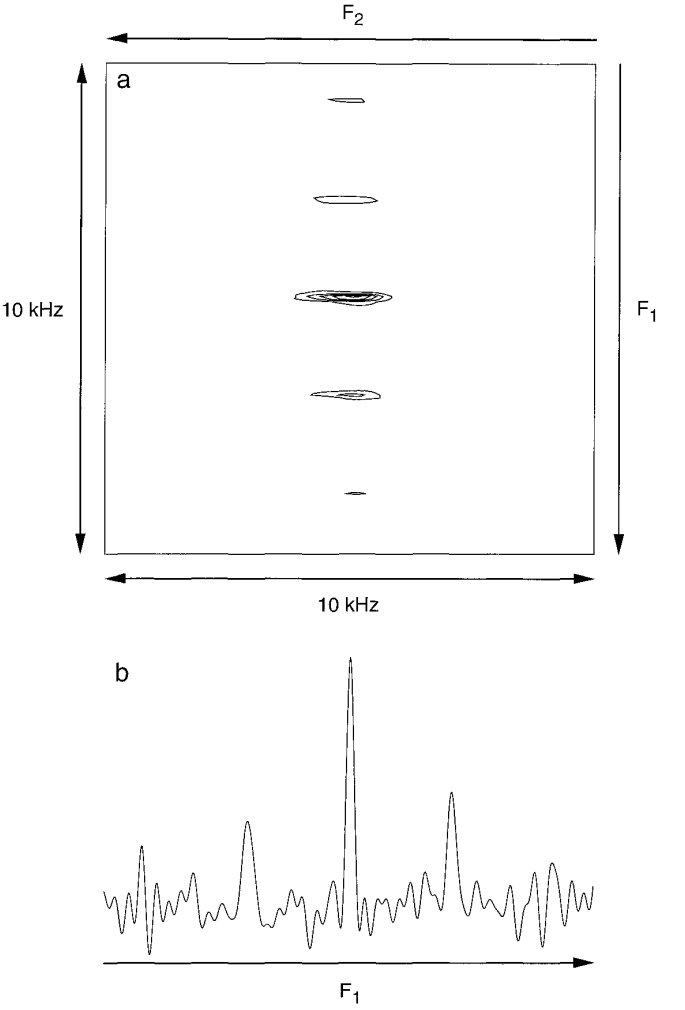

FIG. 5. Two-dimensional triple-quantum MAS ^{27}Al NMR spectrum of albite, $NaSi_3AlO_8$, recorded using the experiment in Fig. 1b with $a = 19$ and $b = 12$. The contour plot is shown in (a) and the projection onto F_1 in (b). The full F_1 and F_2 spectral widths were 10 and 62.5 kHz, 96 transients (consisting of 256 points each) were averaged for each of the 128 increments of t_1, and the relaxation interval was 1 s. Total experiment duration was ~4 hours. The length of the triple-quantum excitation pulse was 7.5 μs, of the $p = +3$ to $+1$ transfer pulse was 1.5 μs, and of the selective refocusing pulse was 7.5 μs. The τ period was 1.11 ms ($6 \times$ rotor period). The data were zero filled to 1024 points in t_1 and 512 points in t_2 prior to Fourier transformation.

MAS ^{27}Al NMR spectrum of the albite sample recorded using the experiment in Fig. 1b (with selection of the dashed coherence pathways). The data were processed in the same fashion as that in Fig. 4.

It should be noted that the new experiments presented in this Communication are formally equivalent to those of Massiot *et al.* (*6*), differing only in their modulation as a function of t_1. For example, a data set recorded using the experiment in Fig. 1a can be converted into a form identical to that which would be obtained with the experiment in Fig. 1b by (i) time shifting the free-induction decays so that all the echoes are aligned and then (ii) deleting the unwanted noise from either side of the echoes. This time shifting of the echoes is, of course, exactly analogous to the t_1-dependent first-order phase correction used by Grandinetti *et al.* (*12*) and Massiot *et al.* (*6*) to shear their spectra. However, we believe that it is preferable to record the data in a format that leads directly to the desired form of spectrum with the minimum of computational manipulation. As a result of the formal equivalence, there is no difference between the two approaches in terms of sensitivity and resolution. This assumes, however, that, with the experiment of Fig. 1a, an additional processing step is introduced to remove the extra noise acquired during the longer t_2 period. The approach described in this Communication to multiple-quantum MAS experiments is also applicable to DAS experiments (*12*) and to the ''hypercomplex'' whole-echo experiment of Massiot *et al.* (*6*).

A full discussion of multiple-quantum MAS experiments with split multiple-quantum/single-quantum evolution (t_1) periods, including further theory, simulations, and experiments, will be presented elsewhere.

ACKNOWLEDGMENTS

Generous support by the Royal Society is acknowledged. We are very grateful to Paul Hodgkinson, who wrote the two-dimensional Fourier transformation program used to process the data shown here, to Monica Price for the sample of albite, and to Stephen Heyes and Mark Simpson for help and encouragement. The MSL 400 spectrometer was purchased with the aid of a grant from the Science and Engineering Research Council. S.P.B. thanks the Engineering and Physical Sciences Research Council and Courtaulds Research for the award of a CASE studentship.

REFERENCES

1. L. Frydman and J. S. Harwood, *J. Am. Chem. Soc.* **117,** 5367 (1995).
2. A. Medek, J. S. Harwood, and L. Frydman, *J. Am. Chem. Soc.* **117,** 12,779 (1995).
3. C. Fernandez and J. P. Amoureux, *Chem. Phys. Lett.* **242,** 449 (1995).
4. C. Jäger, K. Herzog, B. Thomas, M. Feike, and G. Kunath-Fandrei, *Solid State NMR* **5,** 51 (1995).
5. C. Fernandez and J. P. Amoureux, *Solid State NMR* **5,** 315 (1996).
6. D. Massiot, B. Touzo, D. Trumeau, J. P. Coutures, J. Virlet, P. Florian, and P. J. Grandinetti, *Solid State NMR* **6,** 73 (1996).
7. G. Wu, D. Rovnyak, B. Sun, and R. G. Griffin, *Chem. Phys. Lett.* **249,** 210 (1996).
8. S. P. Brown, S. J. Heyes, and S. Wimperis, *J. Magn. Reson. A* **119,** 280 (1996).
9. A. Samoson, E. Lippmaa, and A. Pines, *Mol. Phys.* **65,** 1013 (1988).
10. A. Llor and J. Virlet, *Chem. Phys. Lett.* **152,** 248 (1988).
11. K. T. Mueller, B. Q. Sun, G. C. Chingas, J. W. Zwanziger, T. Terao, and A. Pines, *J. Magn. Reson.* **86,** 470 (1990).
12. P. J. Grandinetti, J. H. Baltisberger, A. Llor, Y. K. Lee, U. Werner, M. A. Eastman, and A. Pines, *J. Magn. Reson. A* **103,** 72 (1993).
13. P. T. Callaghan, ''Principles of Nuclear Magnetic Resonance Microscopy,'' Clarendon Press, Oxford, 1991.
14. G. Bodenhausen, H. Kogler, and R. R. Ernst, *J. Magn. Reson.* **58,** 370 (1984).
15. S. P. Brown and S. Wimperis, *Chem. Phys. Lett.* **237,** 509 (1995).
16. R. M. Bracewell, ''The Fourier Transform and its Applications,'' McGraw–Hill, New York, 1965.
17. A. Wokaun and R. R. Ernst, *J. Chem. Phys.* **67,** 1752 (1977).
18. S. Vega and Y. Naor, *J. Chem. Phys.* **75,** 75 (1981).
19. J. P. Amoureux, *Solid State NMR* **2,** 83 (1993).
20. D. J. States, R. A. Haberkorn, and D. J. Ruben, *J. Magn. Reson.* **48,** 286 (1982).
21. D. Marion and K. Wüthrich, *Biochem. Biophys. Res. Commun.* **113,** 967 (1983).